

ABSOLUTE PROPERTIES OF THE HIGHLY ECCENTRIC ECLIPSING BINARY STAR LV HERCULIS

GUILLERMO TORRES¹, CLAUD H. SANDBERG LACY², ANTONIO CLARET³

Draft version September 11, 2018

ABSTRACT

We report extensive spectroscopic and differential *V*-band photometric observations of the 18.4-day detached double-lined eclipsing binary LV Her (F9 V), which has the highest eccentricity ($e \simeq 0.613$) among the systems with well-measured properties. We determine the absolute masses and radii of the components to be $M_1 = 1.193 \pm 0.010 M_\odot$, $M_2 = 1.1698 \pm 0.0081 M_\odot$, $R_1 = 1.358 \pm 0.012 R_\odot$, and $R_2 = 1.313 \pm 0.011 R_\odot$, with fractional errors of 0.9% or better. The effective temperatures are 6060 ± 150 K and 6030 ± 150 K, respectively, and the overall metallicity is estimated to be $[m/H] = +0.08 \pm 0.21$. A comparison with current stellar evolution models for this composition indicates an excellent fit for an age between 3.8 and 4.2 Gyr, with both stars being near the middle of their main-sequence lifetimes. Full integration of the equations for tidal evolution is consistent with the high eccentricity, and suggests the stars' spin axes are aligned with the orbital axis, and that their rotations should be pseudo-synchronized. The latter prediction is not quite in agreement with the measured projected rotational velocities.

Subject headings: binaries: eclipsing — binaries: spectroscopic — stars: evolution — stars: fundamental parameters — stars: individual (LV Her)

1. INTRODUCTION

The photometric variability of the eclipsing binary star LV Her (TYC 2076-1042-1; $\alpha = 17^{\text{h}} 35^{\text{m}} 32^{\text{s}}.40$, $\delta = +23^\circ 10' 30''.6$, J2000.0; SpT F9, $V = 11.02$) was announced by Hoffmeister (1935). Its period was estimated by Zessewitsch (1944) as 2.634 days, by Zessewitsch (1954) as 5.2674 days, by Popper (1996) as 9.218 days, by Torres (2000) as 18.1312 days, and by Torres et al. (2001) as 18.4359350 days. All photometric and spectroscopic work performed since this last study has confirmed that it is basically correct. The prior erroneous period values resulted from the very long orbital period, the similar eclipse depths (0.68 mag and 0.66 mag in *V*; see below), the extremely high eccentricity of the orbit (0.613), and the resultant shift of secondary eclipse to a phase of 0.86. This sort of erroneous period estimation is not unusual in this kind of situation (Lacy et al. 2004a,b, 2006).

Largely because of this uncertainty, no determination of the absolute dimensions of the system has been made until now. In addition to an accurate determination of the eclipse ephemeris in §2.2, this work presents new high-quality photometric and spectroscopic observations (§2.1 and §2.3) that yield masses and radii on a par with the best determinations for eclipsing binaries to date (§4). In §5.1 we compare these determinations with models of stellar structure and stellar evolution. The high eccentricity and long period of LV Her make it an interesting case for comparison with tidal theory, which we present in §5.2. We discuss our results in §6.

2. OBSERVATIONS AND REDUCTIONS

2.1. Differential and absolute photometry

Our photometric work on LV Her began in 2001 and is based on observations obtained with two robotic instruments: the URSA telescope at Kimpel Observatory (Lacy et al. 2001) on the campus of the University of Arkansas, and a robotic telescope at the NF Observatory (NFO; Grauer et al. 2008) near Silver City, NM.

Kimpel Observatory (ursa.uark.edu) consists of a Meade 10-inch f/6.3 LX-200 telescope with a Santa Barbara Instruments Group ST8 CCD camera (binned 2×2 to produce 765×510 pixel images with 2.3 arcsec square pixels) inside a Technical Innovations Robo-Dome, and controlled automatically by an Apple Macintosh G4 computer. The observatory is located on top of Kimpel Hall on the Fayetteville campus of the University of Arkansas, with the control room directly beneath the observatory inside the building. Exposures of 60 or 120 seconds made through a Bessell *V* filter (2.0 mm of GG 495 and 3.0 mm of BG 39) were read out and downloaded by ImageGrabber (camera control software written by J. Sabby) to the control computer over a 30 second interval, then the next exposure was begun. The observing cadence was therefore about 90 to 150 sec per observation. The variable star would sometimes be monitored continuously for 4–6 hours. LV Her was observed by URSA on 156 nights during parts of nine observing seasons from 2001 February 18 to 2009 April 8. The total number of URSA observations is 6690. The frames were analyzed by a virtual measuring engine application written by Lacy that flat-fielded the images, automatically located the variable and comparison stars in the image, measured their brightnesses, subtracted the corresponding sky brightness, and corrected for the differences in airmass between the stars. Extinction coefficients were determined nightly from the comparison star measurements. They averaged 0.25 mag/airmass. LV Her is TYC 2076-1042-1. The comparison stars were TYC 2076-0580-1 (comp, $V_T = 11.12$, as listed in the Tycho-2 Catalogue; Høg et al. 2000), and TYC 2076-1387-1 (ck, $V_T = 11.53$). Both comparison

¹ Harvard-Smithsonian Center for Astrophysics, 60 Garden St., Cambridge, MA 02138, USA; e-mail: gtorres@cfa.harvard.edu

² Department of Physics, University of Arkansas, Fayetteville, AR 72701, USA; e-mail: clacy@uark.edu

³ Instituto de Astrofísica de Andalucía, CSIC, Apartado 3004, 18080 Granada, Spain; e-mail: claret@iaa.es

TABLE 1
URSA DIFFERENTIAL V -BAND MAGNITUDES OF
LV HER.

HJD-2,440,000	ΔV	Orbital phase
51958.87391 ...	-0.195	0.15136
51958.87498 ...	-0.147	0.15141
51958.87603 ...	-0.174	0.15147
51958.87708 ...	-0.179	0.15153
51958.87812 ...	-0.183	0.15158

NOTE. — Table 1 is available in its entirety in the electronic edition of the *Astronomical Journal*. A portion is shown here for guidance regarding its form and contents.

TABLE 2
NFO DIFFERENTIAL V -BAND MAGNITUDES
OF LV HER.

HJD-2,440,000	ΔV	Orbital phase
53430.93043 ...	1.003	0.99840
53430.93323 ...	1.010	0.99855
53430.93602 ...	1.035	0.99870
53430.93878 ...	1.055	0.99885
53430.94158 ...	1.068	0.99900

NOTE. — Table 2 is available in its entirety in the electronic edition of the *Astronomical Journal*. A portion is shown here for guidance regarding its form and contents.

stars are within 10 arcmin of the variable star (var). The comparison star magnitude differences (comp-ck) were constant at the level of 0.013 mag (standard deviation within a night), and 0.010 mag for the standard deviation of the nightly mean magnitude difference. The URSA differential magnitude (var-comp) of the variable star was referenced only to the magnitude of the comparison star, comp. The resulting 6690 V magnitude differences (var-comp) are listed in Table 1 (without any nightly corrections) and plotted in Figures 1–3 (after the nightly corrections discussed below have been applied). The eclipse depths are 0.68 mag for the primary and 0.66 mag for the secondary. The precision of the variable star differential magnitudes is about 0.016 mag.

The other telescope we used is the NFO WebScope, a refurbished 24-inch Group 128 Cassegrain reflector with a $2K \times 2K$ Kodak CCD camera, located near Silver City, NM. Observations consisted of 120 second exposures also through a Bessell V filter. LV Her was observed by NFO on 123 nights during parts of five observing seasons from 2005 March 1 to 2009 April 24, yielding 2946 observations. Extinction coefficients were determined nightly from the comparison star measurements. They averaged 0.18 mag/airmass. The same comparison stars were used as those of the URSA telescope. The comparison star magnitude differences (comp-ck) were constant at the level of 0.007 mag (standard deviation within a night), and 0.020 mag for the standard deviation of the nightly mean magnitude difference. The differential magnitude (var-comps) of the variable star was referenced to the magnitude corresponding to the sum of the intensities of the comparison star, comp, and the check star, ck. The resulting 2946 V magnitude differences (var-comps) are listed in Table 2 (without nightly corrections) and plot-

ted in Figure 1–3 (including nightly corrections; see below). The precision of the variable star differential magnitudes is about 0.010 mag. We noticed early on during the observations that the NFO magnitudes showed a small but significant offset from night to night, on the order of a hundredth of a magnitude. The origin of the offset is a variation in responsivity across the field of view of the NFO combined with imprecise centering from night to night. These variations are a well-known effect of the optics when using wide-field imaging telescopes such as the NFO. We have removed most of this variation by using dithered exposures of open star clusters to measure this variation, fitting a 2-D polynomial (see Selman 2004), and subtracting the variation during initial reductions (photometric flat). The URSA observations, on the other hand, show this kind of effect to a very much smaller extent. We have removed these nightly offsets before further analysis by using a procedure discussed below in §3.

Absolute photometry of LV Her is available in the literature from several sources, and in several photometric systems including Strömgren, 2MASS, Tycho-2, and Johnson-Cousins. We collect these measurements in Table 3. Color indices formed from these magnitudes can be used to estimate a mean effective temperature for the binary, which we discuss below in §4. The interstellar reddening can be estimated, for example, by comparison with the standard Strömgren indices of Perry & Johnson (1982), giving $E(b-y) = 0.007$ mag, or $E(B-V) \approx 0.01$. Another estimate is available from the reddening maps of the sky near the variable star from Schlegel et al. (1998), which results in a larger value of $E(B-V) = 0.057$ mag

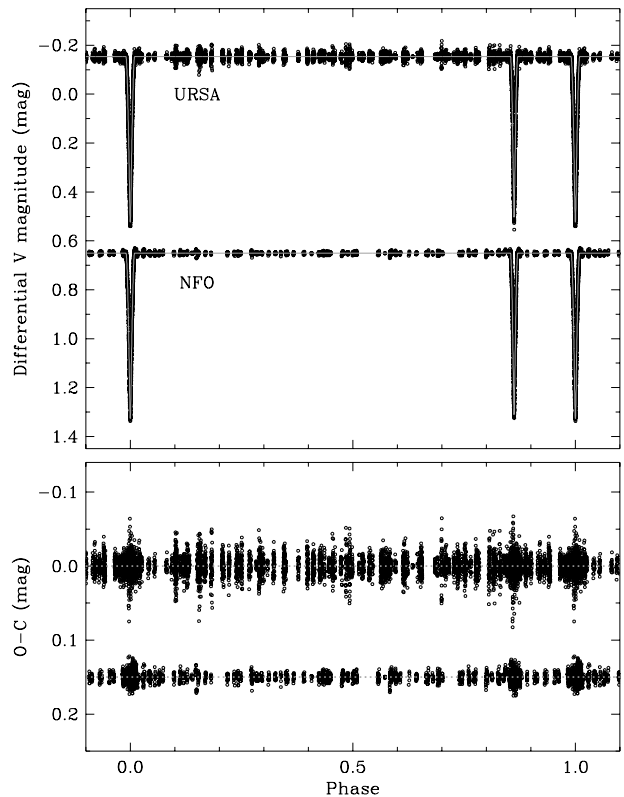


FIG. 1.— URSA and NFO V -band photometry for LV Her, shown with our best fit model described in §3. Residuals are shown at the bottom, with NFO displaced for clarity.

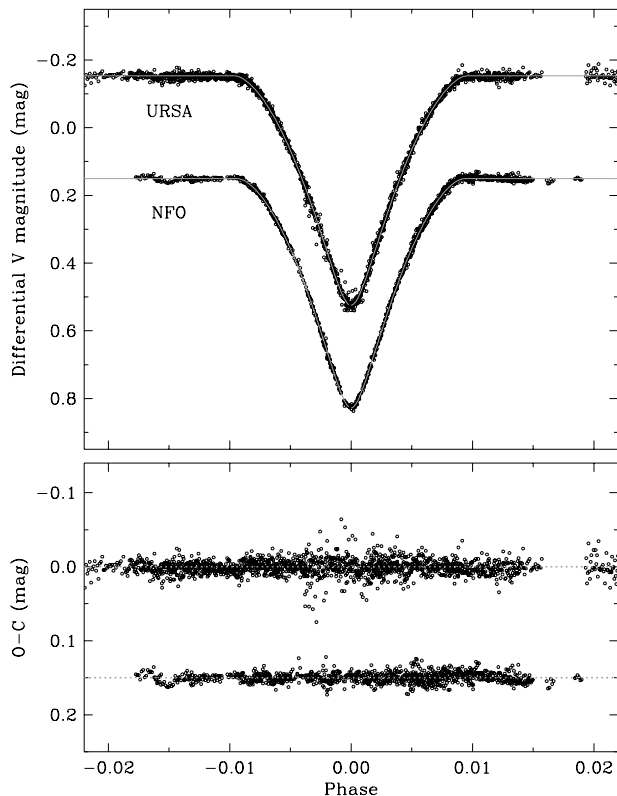


FIG. 2.— Enlarged view of the URSA and NFO V -band light curves for LV Her near the primary eclipse, shown with our best fit model described in §3. Residuals are shown at the bottom, with NFO displaced for clarity.

TABLE 3
ABSOLUTE PHOTOMETRY FOR LV HER (COMBINED LIGHT).

Passband	Value	Reference
y	11.02 ± 0.02^a	1
$u - b$	1.552 ± 0.030^a	1
$v - b$	0.571 ± 0.020^a	1
$b - y$	0.367 ± 0.015^a	1
V	11.055 ± 0.040	2
I_C	10.367 ± 0.058	2
J	9.905 ± 0.018^a	3
H	9.665 ± 0.025^a	3
K_s	9.631 ± 0.018^a	3
BT	11.832 ± 0.066	4
VT	11.045 ± 0.055	4

NOTE. — References: 1 - Hilditch & Hill (1975); 2 - TASS (Droege et al. 2007); 3 - 2MASS; 4 - Tycho-2 (Høg et al. 2000).

^a Single measurement obtained out of eclipse.

at the estimated distance of the eclipsing binary. We adopt for further use the straight average of these two reddening estimates, $E(B - V) = 0.03 \pm 0.03$ mag, with a conservative error.

2.2. Ephemeris

Since the work of Torres et al. (2001), additional times of minimum for LV Her have been reported in the literature, and some recent ones from our WebScopes are available that have not yet been published. The previously published ones and these additional times of minimum

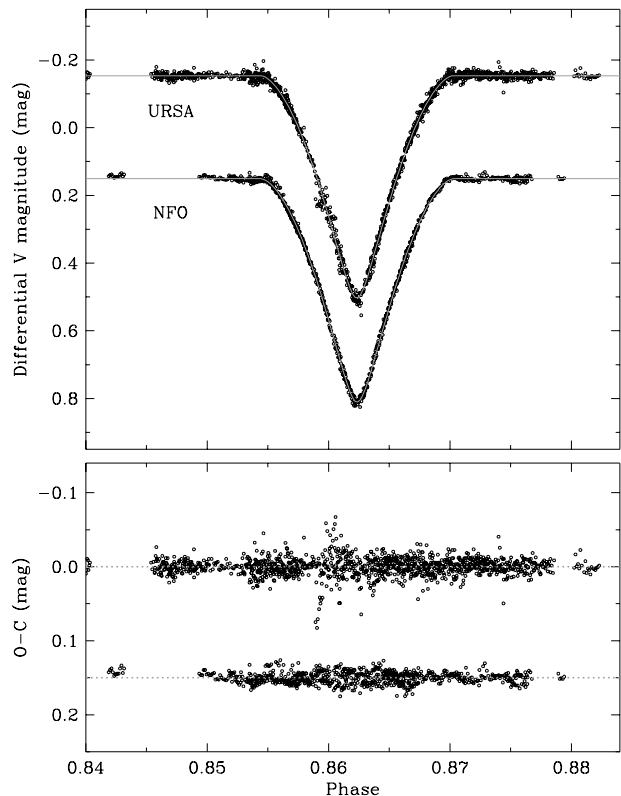


FIG. 3.— Enlarged view of the URSA and NFO V -band light curves for LV Her near the secondary eclipse, shown with our best fit model described in §3. Residuals are shown at the bottom, with NFO displaced for clarity.

light (37 for the primary, 30 for the secondary) are listed in Table 4. All available minima have been used to estimate an eclipse ephemeris by a least squares technique. When available, the uncertainties have been adopted as published. For the others (visual and photographic measurements), uncertainties have been estimated by iterations requiring the reduced χ^2 to be near unity, separately for each class of measurement technique. For the visual measurements we obtain $\sigma = 0.017$ days, and for the photographic timings $\sigma = 0.053$ days. Separate solutions with the primary and secondary data give periods that are not significantly different. For the final ephemeris we enforced a common period, and obtained:

$$\text{Min I} = 2,453,652.19147(10) + 18.4359535(19)E$$

$$\text{Min II} = 2,454,165.86045(12) + 18.4359535(19)E$$

where the reference epochs were chosen so as to minimize the correlations with the period and with each other. This ephemeris is the basis of the orbital phases we cite below. The phase of secondary eclipse is 0.86235 ± 0.00001 . A plot of the $O - C$ diagram from this fit is shown in Figure 4, and the residuals are included in Table 4. It is quite remarkable how much the accuracy has improved over the last century.

2.3. Spectroscopy

LV Her was placed on the observing list at the Harvard-Smithsonian Center for Astrophysics (CfA) on 1991 May 31st, and was monitored spectroscopically for exactly 11 years with an echelle instrument on the 1.5m Tillinghamast reflector at the F. L. Whipple Observatory on

TABLE 4
TIMES OF ECLIPSE FOR LV HER.

HJD-2,400,000	Year	Type	Instrument	σ (d)	$O-C$ (d)	Reference
15929.712	1902.4907	2	pg	0.053	+0.01915	1
16224.798	1903.2986	2	pg	0.053	+0.12989	1
16669.658	1904.5165	1	pg	0.053	-0.01072	1
17351.799	1906.3841	1	pg	0.053	-0.00000	1
18605.473	1909.8165	1	pg	0.053	+0.02916	1
23601.681	1923.4954	1	pg	0.053	+0.09376	1
24062.505	1924.7570	1	pg	0.053	+0.01892	1
26032.643	1930.1510	2	pg	0.053	+0.04762	1
26032.644	1930.1510	2	pg	0.053	+0.04862	1
26090.482	1930.3093	1	pg	0.053	+0.04103	1
26219.577	1930.6628	1	pg	0.053	+0.08436	1
26901.699	1932.5303	1	pg	0.053	+0.07608	1
27212.514	1933.3813	2	pg	0.053	+0.01760	1
27636.462	1934.5420	2	pg	0.053	-0.06134	1
27657.429	1934.5994	1	pg	0.053	-0.06802	1
28281.830	1936.3089	2	pg	0.053	+0.04829	1
28429.2740	1936.7126	2	vis	0.017	+0.00466	2
28487.1220	1936.8710	1	vis	0.017	+0.00708	2
30254.522	1941.7098	2	pg	0.053	+0.09326	1
31268.42	1944.4857	2	vis	0.017	+0.01382	3
31289.35	1944.5431	1	vis	0.04	-0.02986	3
31326.29	1944.6442	1	vis	0.017	+0.03823	3
31342.16	1944.6876	2	vis	0.017	+0.01001	3
34626.332	1953.6792	1	pg	0.053	+0.04456	1
37444.539	1961.3950	2	pg	0.053	+0.08839	1
38147.573	1963.3198	1	pg	0.053	+0.01843	1
38587.449	1964.5242	2	pg	0.053	-0.03072	1
40744.498	1970.4298	2	pg	0.053	+0.01171	1
41060.502	1971.2950	1	pg	0.053	+0.06678	1
41982.251	1973.8186	1	pg	0.053	+0.01810	1
42664.347	1975.6861	1	pg	0.053	-0.01618	1
46001.268	1984.8221	1	pg	0.053	-0.00276	1
46941.483	1987.3963	1	pg	0.053	-0.02139	1
47381.384	1988.6006	2	pg	0.053	-0.04555	1
48100.425	1990.5693	2	pg	0.053	-0.00674	1
48487.60	1991.6293	2	vis	0.017	+0.01328	1
48508.60	1991.6868	1	vis	0.04	+0.03956	1
48545.52	1991.7879	1	vis	0.04	+0.08765	1
48745.70	1992.3359	2	vis	0.017	+0.00989	1
48948.50	1992.8912	2	vis	0.017	+0.01440	1
49098.540	1993.3020	1	pg	0.053	+0.02904	1
49206.61	1993.5978	2	vis	0.017	+0.02105	1
49667.49	1994.8597	2	vis	0.017	+0.00221	1
49688.48	1994.9171	1	vis	0.017	+0.01853	1
49925.65	1995.5665	2	vis	0.02	+0.05886	1
52008.85	2001.2700	2	ccd	0.01	-0.00388	1
52045.74	2001.3710	2	ccd	0.01	+0.01421	1
52066.6993	2001.4283	1	ccd	0.0008	-0.00017	1
52432.88040	2002.4309	2	ccd	0.00050	-0.00042	4*
52490.72613	2002.5893	1	ccd	0.00020	-0.00027	4
52785.7012	2003.3969	1	ccd	0.0010	-0.00046	5
53154.4210	2004.4064	1	ccd	0.0017	+0.00027	6
53154.4212	2004.4064	1	ccd	0.0015	+0.00047	6
53209.7288	2004.5578	1	ccd	0.0004	+0.00021	7
53430.95992	2005.1635	1	ccd	0.00016	-0.00011	8
53870.8862	2006.3679	2	ccd	0.0005	+0.00101	9*
53907.7573	2006.4689	2	ccd	0.0002	+0.00020	9
53928.7308	2006.5263	1	ccd	0.0003	+0.00002	9
54297.44944	2007.5358	1	ccd	0.00040	-0.00041	10
54297.4498	2007.5358	1	ccd	0.0008	-0.00005	11
54297.4509	2007.5358	1	ccd	0.0004	+0.00105	12
54331.7839	2007.6298	2	ccd	0.0003	-0.00013	13
54368.6555	2007.7307	2	ccd	0.0003	-0.00043	13
54589.8873	2008.3364	2	ccd	0.0002	-0.00008	13
54647.7328	2008.4948	1	ccd	0.0006	-0.00016	13
54647.7332	2008.4948	1	ccd	0.0002	+0.00024	13
54868.9645	2009.1005	1	ccd	0.0007	+0.00010	13

NOTE. — Type: 1 = primary, 2 = secondary. Instrument: pg = photographic, vis = visual, ccd = CCD. References: 1 - Torres et al. (2001); 2 - Variable Star and Exoplanet Section of the Czech Astronomical Society (http://var2.astro.cz/EN/brno/eclipsing_binaries.php); 3 - Zesewitsch (1954); 4 - Lacy (2002); 5 - Lacy (2003); 6 - Hübscher (2005); 7 - Lacy (2004); 8 - Lacy (2006); 9 - Lacy (2007); 10 - Brát et al. (2007); 11 - Hübscher et al. (2008); 12 - Diethelm (2008); 13 - This paper; * - Remeasurement.

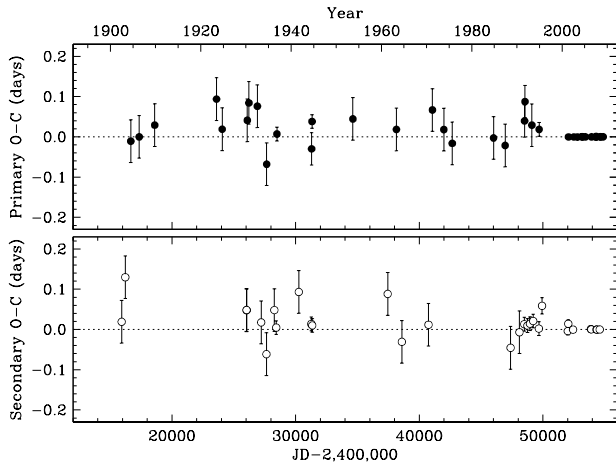


FIG. 4.— Residuals from our fit to the primary and secondary eclipse timings of LV Her given in Table 4.

Mount Hopkins, Arizona. We collected 42 spectra with a photon-counting intensified Reticon detector (Latham 1985, 1992) in a single order 45 \AA wide centered near 5187 \AA . The main features in this spectral window are the lines of the Mg I b triplet. The resolving power provided by this setup is $\lambda/\Delta\lambda \approx 35,000$. Two additional observations, for a total of 44, were obtained with a nearly identical system on the 1.5m Wyeth reflector at the Oak Ridge Observatory (Harvard, Massachusetts). The signal-to-noise ratios of these spectra range from 13 to 28 per resolution element of 8.5 km s^{-1} .

Radial velocities for the two components were derived using TODCOR, a two-dimensional cross-correlation technique (Zucker & Mazeh 1994). This method uses two templates, one for each component of the binary, which we selected from a large library of synthetic spectra based on model atmospheres by R. L. Kurucz (see Latham et al. 2002). These templates have been calculated for a wide range of effective temperatures (T_{eff}), surface gravities ($\log g$), rotational velocities ($v \sin i$ when seen in projection), and metallicities ($[m/H]$). Following Torres et al. (2002) the optimum templates for each star were determined by means of extensive grids of cross-correlations with TODCOR, seeking to maximize the average correlation weighted by the strength of each exposure. Because of the strong correlation between temperature, surface gravity, and metallicity in our narrow spectral window, we initially assumed solar metallicity, and surface gravities of $\log g = 4.0$ for both components, close to the values determined from a preliminary analysis. The projected rotational velocities we obtained are $v \sin i = 13 \pm 1 \text{ km s}^{-1}$ for both stars, and the best-fit temperatures were near solar, with a difference of only 20–30 K between the primary and secondary. For the radial velocity measurements we adopted $T_{\text{eff}} = 5750 \text{ K}$. In § 4 we describe experiments in which we extended the grids of correlations to other compositions in order to fine-tune the temperatures and attempt to constrain the metallicity. These minor changes in the stellar parameters have no effect on the radial velocities. Typical errors for our measurements are 0.8 km s^{-1} for the primary and 1.1 km s^{-1} for the secondary. The stability of the zero-point of the CfA velocity system was monitored by means of exposures of the dusk and dawn sky, and

TABLE 5
SPECTROSCOPIC ORBITAL SOLUTION FOR LV HER.

Parameter	Value
Adjusted quantities	
P (days) ^a	18.4359535
T_1 (HJD–2,400,000) ^a	53,652.19147
K_1 (km s^{-1})	67.24 ± 0.19
K_2 (km s^{-1})	68.59 ± 0.27
γ (km s^{-1})	-10.278 ± 0.094
e	0.61273 ± 0.00073
ω (deg)	352.20 ± 0.24
Derived quantities	
$M_1 \sin^3 i$ (M_\odot)	1.193 ± 0.010
$M_2 \sin^3 i$ (M_\odot)	1.1697 ± 0.0080
$q \equiv M_2/M_1$	0.9803 ± 0.0047
$a_1 \sin i$ (10^6 km)	13.471 ± 0.037
$a_2 \sin i$ (10^6 km)	13.743 ± 0.054
$a \sin i$ (R_\odot)	39.119 ± 0.095
Other quantities pertaining to the fit	
N_{obs}	44
Time span (days)	4018.0
σ_1 (km s^{-1})	0.76
σ_2 (km s^{-1})	1.10

^a Ephemeris adopted from § 2.2.

small systematic run-to-run corrections were applied in the manner described by Latham (1992). We determined also the light ratio directly from our spectra following Zucker & Mazeh (1994), and obtained $\ell_2/\ell_1 = 0.95 \pm 0.03$ at the mean wavelength of our observations, which is essentially also the ratio in the visual band given that the stars are nearly identical in temperature.

Although TODCOR significantly reduces systematic

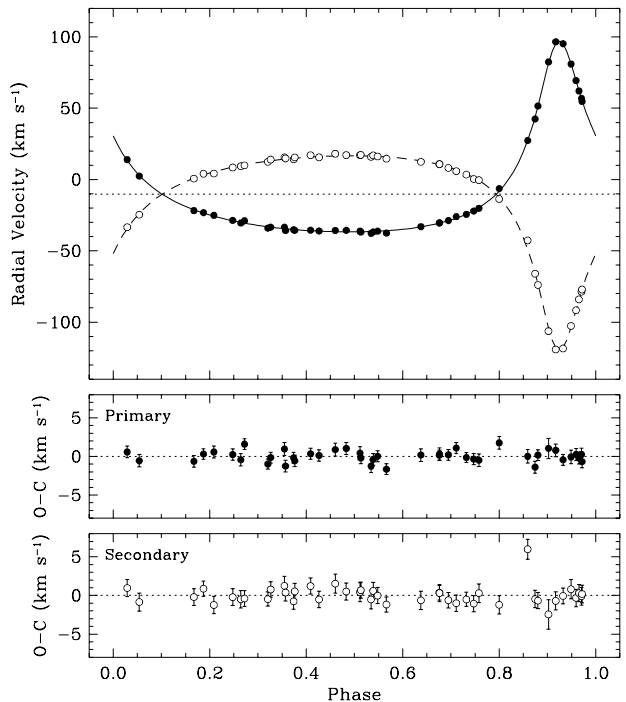


FIG. 5.— Radial-velocity measurements for LV Her (filled circles for the primary, open for the secondary) along with the curves computed from our orbital solution. Phase 0.0 corresponds to the time of primary eclipse. The dotted line represents the velocity of the center of mass, and the error bars are smaller than the symbol size. O–C residuals for the primary and secondary are shown in the bottom panels.

TABLE 6
RADIAL VELOCITY MEASUREMENTS OF LV HER.

HJD (2,400,000+)	RV_1 (km s ⁻¹)	RV_2 (km s ⁻¹)	σ_1 (km s ⁻¹)	σ_2 (km s ⁻¹)	$(O-C)_1$ (km s ⁻¹)	$(O-C)_2$ (km s ⁻¹)	Phase
48407.8794	-36.77	+16.94	0.75	1.09	-0.38	+0.59	0.5389
48428.8481	-30.28	+10.75	0.77	1.12	+0.32	+0.30	0.6763
48435.8126	+2.41	-24.64	0.81	1.17	-0.56	-0.85	0.0541
48459.7950	-33.43	+15.58	0.84	1.22	+0.97	+1.25	0.3549
48461.7375	-35.70	+18.08	0.85	1.23	+0.88	+1.53	0.4603
48462.6830	-36.20	+17.06	0.84	1.22	+0.44	+0.44	0.5116
51709.7370	-33.05	+12.51	0.82	1.19	+0.18	-0.62	0.6377
51710.7867	-28.71	+8.12	0.69	1.00	+0.21	-0.61	0.6947
51711.7546	-22.10	+0.39	0.72	1.04	-0.34	-1.05	0.7472
51712.7284	-6.38	-13.66	0.81	1.18	+1.76	-1.20	0.8000
51715.7770	+62.12	-84.03	0.77	1.11	-0.20	+0.31	0.9653
51740.7610	-34.04	+12.50	0.64	0.93	-0.98	-0.46	0.3205
51741.7446	-35.18	+14.19	0.72	1.04	-0.18	-0.75	0.3739
51742.7170	-36.06	+15.62	0.74	1.07	+0.12	-0.52	0.4266
51744.7057	-37.70	+15.90	0.83	1.21	-1.26	-0.51	0.5345
51799.6219	-36.83	+17.30	0.73	1.05	-0.20	+0.69	0.5132
51800.6010	-37.55	+14.68	0.69	1.00	-1.65	-1.17	0.5663
51802.6229	-30.48	+10.83	0.66	0.95	+0.14	+0.36	0.6760
51803.6558	-24.42	+3.48	0.64	0.92	-0.15	-0.51	0.7320
51831.5984	-28.65	+8.50	0.75	1.08	+0.24	-0.21	0.2477
51833.6157	-35.73	+14.79	0.75	1.09	-1.25	+0.38	0.3571
51834.5731	-35.52	+17.04	0.72	1.04	+0.34	+1.22	0.4091
51858.5764	-26.02	+5.88	0.73	1.06	+1.09	-1.01	0.7110
51861.5870	+42.50	-66.00	0.77	1.12	-1.39	-0.46	0.8743
51973.9772	+56.88	-78.61	0.79	1.14	+0.26	-0.09	0.9706
51977.9683	-23.19	+4.08	0.68	0.98	+0.30	+0.88	0.1871
52006.9280	-20.18	-0.38	0.83	1.21	-0.49	+0.30	0.7579
52009.8622	+96.55	-119.15	0.81	1.18	+0.79	-0.70	0.9171
52010.8700	+54.74	-77.11	0.80	1.16	-0.68	+0.19	0.9717
52011.9261	+13.95	-33.43	0.76	1.10	+0.58	+0.97	0.0290
52032.9120	-21.81	+0.64	0.75	1.09	-0.63	-0.20	0.1673
52034.8450	-28.93	+9.98	0.71	1.04	+1.59	-0.39	0.2722
52035.8449	-33.46	+14.00	0.70	1.02	-0.15	+0.78	0.3264
52039.9325	-36.23	+16.20	0.73	1.05	+0.02	-0.01	0.5481
52102.6290	+80.99	-102.64	0.87	1.26	-0.07	+0.81	0.9489
52138.6401	+82.46	-106.28	1.31	1.91	+1.04	-2.45	0.9022
52156.6725	+51.60	-73.90	0.71	1.04	+0.17	-0.67	0.8803
52157.6303	+95.25	-118.44	0.70	1.01	-0.44	-0.06	0.9323
52211.5883	+27.39	-42.70	0.89	1.30	+0.01	+5.99	0.8590
52360.9241	+69.40	-91.63	0.78	1.13	+0.24	-0.31	0.9593
52420.8295	-25.10	+4.20	0.77	1.11	+0.58	-1.23	0.2087
52421.8579	-30.47	+9.39	0.78	1.13	-0.43	-0.49	0.2645
52423.9196	-35.64	+15.54	0.73	1.06	-0.57	+0.53	0.3763
52425.8862	-35.66	+17.17	0.77	1.11	+1.03	+0.51	0.4830

NOTE. — Radial velocities are in the heliocentric frame, and include all corrections described in the text.

errors in the radial velocities caused by line blending, residual effects can remain as a result of shifts of the spectral lines in and out of our narrow spectral window as a function of orbital phase. We investigated these effects by means of numerical simulations similar to those described by Latham et al. (1996) (see also Torres et al. 1997, 2000a). We generated synthetic composite spectra matching our observations by combining copies of the primary and secondary templates used above, shifted to the appropriate velocities for each of the exposures as predicted by a preliminary orbital solution, and scaled to the observed light ratio. These synthetic observations were then processed with TODCOR in exactly the same way as the real spectra, and the resulting velocities were compared with the input shifts. The differences for LV Her were typically well under 0.5 km s⁻¹ for both stars, but were nevertheless applied as corrections to the raw velocities. They affect the masses at the level of 1.3% for the primary and 0.8% for the secondary, which are similar to the formal errors. The corrected measurements are

listed in Table 6 along with their uncertainties. Similar adjustments based on the same simulations were made to the light ratio, and are already included in the value reported above.

Our orbital solution is shown in Figure 5, and was derived holding the ephemeris fixed according to § 2.2. The residuals are shown as well, and are listed in Table 6. The orbital elements and derived quantities (minimum masses, semimajor axes, etc.) are given in Table 5.

3. MODELING OF THE PHOTOMETRIC OBSERVATIONS

In order to remove the small nightly offsets in the differential photometry, we performed preliminary fits of the URSA and NFO light curves by using the Nelson-Davis-Etzel model (Popper & Etzel 1981; Etzel 1981) as implemented in the EBOP code. This model is well suited for well-detached systems such as LV Her. The nightly residuals, which were typically less than 0.02 mag and were uncorrelated with phase, were removed from each light curve. This improved the resid-

TABLE 7
PHOTOMETRIC ORBITAL SOLUTIONS FOR LV HER.

Parameter	URSA	NFO	Adopted
J_2	0.967 ± 0.004	0.983 ± 0.003	0.9772 ± 0.0080
$r_1 + r_2$	0.06880 ± 0.00009	0.06806 ± 0.00006	0.06829 ± 0.00037
$k \equiv r_2/r_1$	0.986 ± 0.015	0.961 ± 0.009	0.968 ± 0.012
r_1	0.03465 ± 0.00026	0.03471 ± 0.00015	0.03470 ± 0.00028
r_2	0.03415 ± 0.00026	0.03335 ± 0.00016	0.03357 ± 0.00028
i (deg).....	89.489 ± 0.010	89.509 ± 0.009	89.500 ± 0.010
$e \cos \omega$	0.60662 ± 0.00011	0.60739 ± 0.00006	0.60721 ± 0.00038
$e \sin \omega$	-0.0938 ± 0.0019	-0.0796 ± 0.0012	-0.0836 ± 0.0071
e	0.61383 ± 0.00018	0.61259 ± 0.00010	0.61288 ± 0.00062
ω (deg).....	351.21 ± 0.18	352.53 ± 0.12	352.12 ± 0.66
ℓ_1	0.516 ± 0.007	0.524 ± 0.004	0.5220 ± 0.0040
ℓ_2	0.484 ± 0.007	0.476 ± 0.004	0.4780 ± 0.0040
$(\ell_2/\ell_1)_V$	0.938 ± 0.024	0.908 ± 0.014	0.916 ± 0.015
$u_1 = u_2$	0.53 ± 0.04	0.55 ± 0.04	0.54 ± 0.03
N_{obs}	6690	2946	...
Time span (days)....	2970.9	1514.9	...
σ_V (mmag).....	12.49	6.42	...

uals of the URSA data by about 27%, and those from NFO by a more significant 42%. The corrected light curves were then fitted by using the JKTEBOP code of Southworth et al. (2007), based on the same model, which allows for more realistic estimates of the uncertainties. The adjustable parameters are the central surface brightness J_2 of the secondary relative to the primary, the inclination angle i , the sum of the relative radii $r_1 + r_2$, the ratio of the radii $k \equiv r_2/r_1$, the eccentricity factors $e \cos \omega$ and $e \sin \omega$, a phase shift, and the magnitude at quadrature. A linear limb-darkening law was adopted, consistent with our experience that with the amount and precision of our data, nonlinear laws do not improve the accuracy of the fits significantly (e.g., Lacy et al. 2005, 2008). The coefficient u was left free, and constrained to be the same for the two stars. The gravity brightening exponent was set to 0.35 for both stars, based on the calculations by Claret (1998) and the mean temperature and surface gravity of the components. The mass ratio q was adopted from the spectroscopy.

Separate solutions for the URSA and NFO photometry are given in Table 7. The uncertainties for the fitted parameters were evaluated by Monte Carlo simulation with JKTEBOP. Tests indicated third light was not significant, and it was therefore set to zero. The last column of the table gives the adopted fit (weighted average), with uncertainties that account for the difference between URSA and NFO. The uncertainties for the individual radii were derived following the prescription recommended by Torres et al. (2000b), based on the errors for $r_1 + r_2$ and k . The synthetic curve corresponding to the adopted solution is displayed in Figures 1–3 along with the observations. The eccentricity and ω from the light curves are in excellent agreement with the spectroscopic values in Table 5, and the photometric light ratio $(\ell_2/\ell_1)_V = 0.916 \pm 0.015$ is consistent with the estimate of $\ell_2/\ell_1 = 0.95 \pm 0.03$ from the CfA spectra. The well-detached stars are essentially spherical, and both eclipses are partial, with 88.4% of the primary light blocked at the primary minimum, and 95.6% of the secondary light covered at the secondary minimum.

We note that the linear limb-darkening coefficient we determined, $u = 0.54 \pm 0.03$, is consistent with theo-

retical value of 0.568 for the visual band according to van Hamme (1993), but is significantly smaller than the value 0.658 from the tables by Claret (2000), for a star of this temperature and surface gravity. Similar discrepancies have been found in other systems (see, e.g., Claret 2008). As a test we repeated the light curve fits holding the limb-darkening coefficient fixed at this last theoretical value. The change in $r_1 + r_2$ was only +0.15%, the individual radii increased by less than 0.1%, and the inclination angle decreased by 0.065. These changes do not impact the absolute masses or radii at a significant level, compared to other sources of uncertainty.

4. ABSOLUTE DIMENSIONS

The photometric orbit and the spectroscopic orbit may be combined to yield the absolute masses and radii of the binary stars' components. These are given in Table 8, along with other properties described below. The masses and radii are determined to 0.9% or better for both stars. The tests and checks for systematics described above suggest that they are also accurate at this level.

The ratio of the effective temperatures is very well constrained from the light curves through the central surface brightness parameter J_2 , according to which the stars differ by only about 30 K (Popper 1980, Table 1). A similar difference was obtained from the CfA spectra. The *absolute* temperatures of the stars may in principle be estimated also from the spectroscopy, though in practice this is difficult with the material at hand because of the correlation with metallicity mentioned earlier. We first determined the magnitude of this dependence by repeating the grids of correlations described in § 2.3 for metallicities between $[m/H] = -1.0$ and $[m/H] = +0.5$ in steps of 0.5 dex, and surface gravities of $\log g = 4.0$ and 4.5. At each composition we determined the primary and secondary temperatures interpolated to the surface gravities indicated in Table 8, as well as the luminosity-weighted mean temperature for the system (where the weights depend only on the radius ratio and temperature ratio that come from the light curve fits). An additional constraint on the mean system temperature is available from the absolute photometry of LV Her presented earlier, through color indices and color-temperature calibrations (including metallicity terms). Equating the two

TABLE 8
PHYSICAL PROPERTIES OF LV HER.

Parameter	Primary	Secondary
Mass (M_{\odot})	1.193 ± 0.010	1.1698 ± 0.0081
Radius (R_{\odot})	1.358 ± 0.012	1.313 ± 0.011
$\log g$ (cgs)	4.2493 ± 0.0082	4.2695 ± 0.0081
Temperature (K)	6060 ± 150	6030 ± 150
$\log L$ (L_{\odot})	0.349 ± 0.044	0.311 ± 0.044
M_{bol} (mag)	3.86 ± 0.11	3.95 ± 0.11
BC_V^a	-0.04 ± 0.10	-0.04 ± 0.10
M_V (mag) ^b	3.90 ± 0.16	4.00 ± 0.16
a (R_{\odot})	39.120 ± 0.095	
Distance (pc)	352 ± 24	
[m/H]	$+0.08 \pm 0.21$	
$v \sin i$ (km s^{-1}) ^c	13 ± 1	13 ± 1
$v_{\text{psync}} \sin i$ (km s^{-1}) ^d	16.0 ± 0.1	15.5 ± 0.1
$v_{\text{peri}} \sin i$ (km s^{-1}) ^e	19.6 ± 0.2	19.0 ± 0.2

^a BC_V is taken from Flower (1996), and the uncertainty includes the contribution from the temperature as well as an additional 0.10 mag added in quadrature.

^b The bolometric magnitude adopted for the Sun is $M_{\text{bol}}^{\odot} = 4.732$, for consistency with the zero-point of the bolometric corrections from Flower (1996).

^c Value measured spectroscopically.

^d Projected pseudo-synchronous rotational velocity.

^e Projected synchronous rotational velocity at periastron.

mean temperatures then allows to solve for the metallicity. With the photometry listed in Table 3 we formed 7 different color indices, we de-reddened them as indicated in § 2.1, and we made use of three different calibrations by Ramírez & Meléndez (2005), Casagrande et al. (2006), and González Hernández & Bonifacio (2009). While the 7 indices are not independent, they are useful in providing an idea of the internal consistency of the results. The agreement between the different indices and different calibrations is excellent, generally within 100 K. The metallicity dependence of the photometric temperatures is small, but was nevertheless accounted for by iterations with the spectroscopic results. We obtained a mean system temperature of $T_{\text{eff}} = 6050 \pm 140$ K and $[\text{m}/\text{H}] = +0.08 \pm 0.21$, where the errors are dominated by the uncertain reddening. The primary and secondary temperatures are then 6060 ± 150 K and 6030 ± 150 K, respectively, though of course ΔT_{eff} is known much more precisely. These temperatures correspond to a spectral type of approximately F9 (e.g., Popper 1980).

LV Her does not have an entry in the *Hipparcos* catalog (Perryman et al. 1997). The distance to the system is estimated here as 352 ± 24 pc, based on the bolometric luminosities, the apparent system magnitude of $V = 11.02 \pm 0.02$ (Table 3), the adopted extinction of $3.1 \times E(B - V)$, and bolometric corrections from Flower (1996). Separate distance estimates for each component agree nearly perfectly, showing the internal consistency of the results.

Also listed in Table 8 are the rotational velocities (projected along the line of sight) expected if the stars were pseudo-synchronized (see Hut 1981), as well as those that correspond to synchronization with the angular velocity at periastron, for comparison with the measured $v \sin i$ values. We discuss these below.

5. COMPARISON WITH THEORY

The high accuracy and precision of our measurements for LV Her offers the opportunity to test various aspects

of theoretical modeling. In this particular case, knowledge of the chemical composition, even though the precision is not as high, is especially interesting since it is rarely available for eclipsing binaries and it eliminates one of the free parameters in the comparison with theory.

5.1. Stellar evolution theory

In Figure 6a we compare the two best determined parameters of LV Her (M and R) against model isochrones from the Yonsei-Yale series by Yi et al. (2001), computed for the metallicity of $[\text{Fe}/\text{H}] = +0.08$ determined in § 4. These models include convective core overshooting (see Demarque et al. 2004), which has an effect for stars of this mass and higher, and treats convection in the standard mixing length approximation, with a mixing length parameter $\alpha_{\text{ML}} = 1.7432$, calibrated against the Sun. An isochrone corresponding to 3.85 Gyr (solid line) provides an excellent fit, and the high precision of the measurements suggests an age uncertainty of no more than 0.4 Gyr for this fixed metallicity. However, the relatively large error in the measured $[\text{Fe}/\text{H}]$ adds significantly to the age uncertainty. This is shown by the shaded area around the 3.85 Gyr isochrone corresponding to $\sigma_{[\text{Fe}/\text{H}]} = 0.21$ dex, which contributes at least another 0.5 Gyr. In the lower panel of the figure the temperature is shown as a function of mass, with the same models as in the top panel. Once again the isochrone of 3.85 Gyr matches the observations very well, but in this case the lower precision of T_{eff} provides a much weaker constraint on the age, and gives rise to a larger uncertainty than the error that comes from $[\text{Fe}/\text{H}]$.

The $T_{\text{eff}} - \log g$ diagram in Figure 7 implicitly compares all four measured quantities (M , R , T_{eff} , and $[\text{Fe}/\text{H}]$) against evolutionary tracks from the Yonsei-Yale series. The models are computed for the observed metallicity of $[\text{Fe}/\text{H}] = +0.08$, and for the precise masses we measure. The shaded area indicates the uncertainty in the location of the tracks that comes from the mass errors. The same 3.85 Gyr isochrone as before is shown with a dashed line. The stars are seen to be in the middle of the main-sequence band.

A similarly good fit to the properties of LV Her is provided by the stellar evolution models of Claret (2004), shown in Figure 8, also for a metallicity constrained to the measured value. These models are similar to the ones used before in their treatment of convection ($\alpha_{\text{ML}} = 1.68$), and also include overshooting ($\alpha_{\text{ov}} = 0.20$), but differ in the details. In this case, we find that the best-fit age is 4.2 Gyr, about 9% older than with the Yonsei-Yale models. The difference is of the same order as the age uncertainty discussed above.

5.2. Tidal theory

The high orbital eccentricity and our accurate measurement of the projected rotational velocities of both components constitute useful probes of tidal forces in the system and allow for an interesting comparison with the predictions from theory. For our initial comparisons we have used the radiative damping formalism of Zahn (1977) and Zahn (1989), often invoked for this type of analysis, to calculate the critical times for LV Her corresponding to synchronization of the axial rotations, align-

ment of the rotational and orbital axes, and circularization of the orbit. These are then compared with the evolutionary age, which is 4.2 Gyr according to the models by Claret 2004 used in this section. The procedure

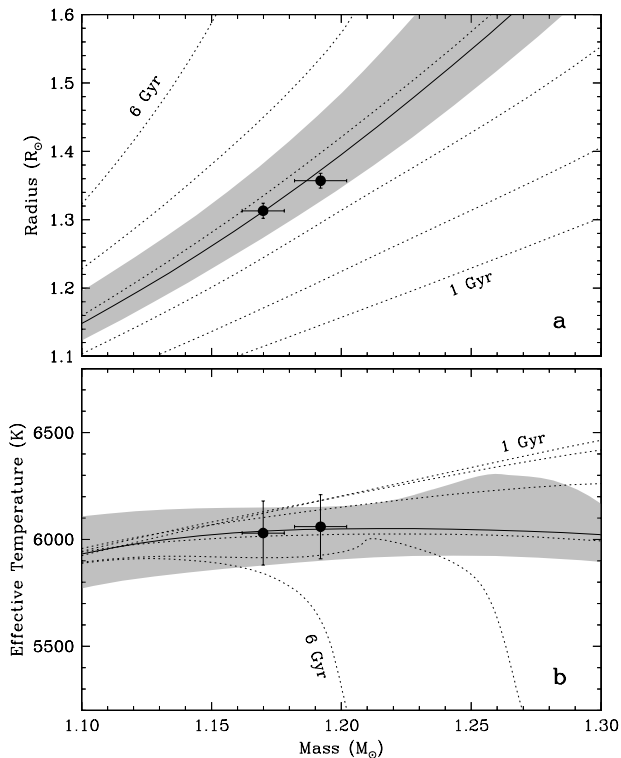


FIG. 6.— Measurements for LV Her compared against the Yonsei-Yale models (Yi et al. 2001; Demarque et al. 2004). (a) Radius vs. mass, shown with isochrones from 1 Gyr to 6 Gyr in steps of 1 Gyr (dotted lines) for a fixed metallicity of $[\text{Fe}/\text{H}] = +0.08$. The best-fit isochrone for 3.85 Gyr is indicated with a solid line. The shaded area indicates the uncertainty that comes from the 0.21 dex error in the measured metallicity, at this particular age. (b) Effective temperature vs. mass.

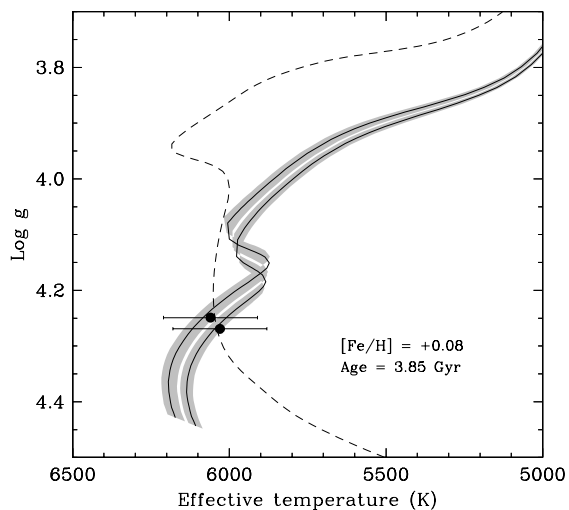


FIG. 7.— Surface gravity vs. effective temperature diagram for LV Her. The solid lines correspond to evolutionary tracks from the Yonsei-Yale series (Yi et al. 2001; Demarque et al. 2004) for the exact masses we measure, and for the observed chemical composition. The effect of the mass uncertainties in the location of these tracks is indicated by the shaded areas. The dashed line represents the best-fit isochrone for 3.85 Gyr.

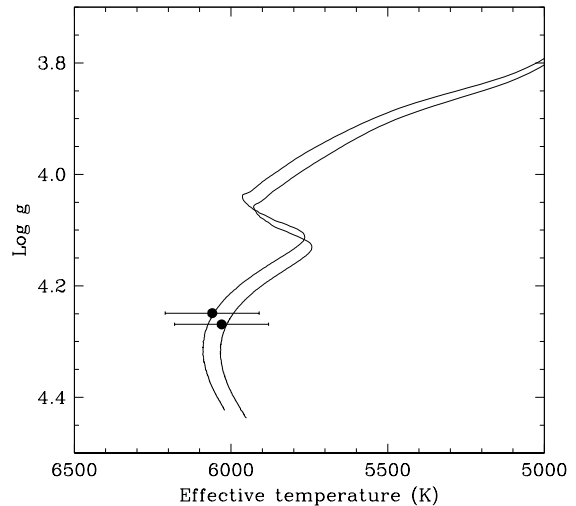


FIG. 8.— Surface gravity vs. effective temperature of LV Her compared with models by Claret (2004). The solid lines correspond to evolutionary tracks for the measured masses, and for the observed chemical composition. The age according to these models is 4.2 Gyr.

follows closely that described by Claret & Cunha (1997), and consists of integrating the differential equations describing the changes in these quantities along the evolutionary track for each star.

We find that rotational synchronization due to tidal forces is not expected to occur for the primary until the system reaches an age of $\tau_{\text{sync},1} = 5.7$ Gyr ($\log \tau_{\text{sync},1} = 9.754$), and the secondary synchronization is predicted to happen shortly after ($\tau_{\text{sync},2} = 5.9$ Gyr, $\log \tau_{\text{sync},2} = 9.774$). This appears to be in agreement with the fact that the measured $v \sin i$ values are slower than expected for pseudo-synchronization in the eccentric orbit (Table 8), assuming the spin axes are parallel to the orbital axis (but see below). The time of orbital circularization indicated by theory is 7.3 Gyr ($\log \tau_{\text{circ}} = 9.862$), again consistent with the fact that the orbit is observed to be highly eccentric. These times are displayed graphically in Figure 9, along with the evolution of the radius of each star according to the evolutionary tracks.

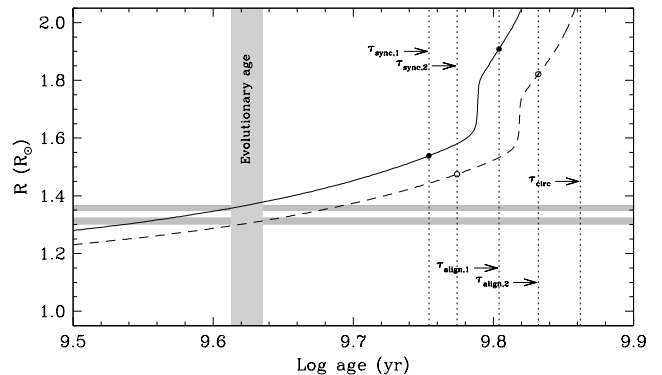


FIG. 9.— Radius as a function of age for LV Her (solid line for the primary, dashed for the secondary) from the stellar evolution models by Claret (2004), for the measured masses and metallicity. Measured radii and their uncertainties are represented by the horizontal shaded bands. The critical times according to the theory by Zahn (1977, 1989) are indicated with arrows for synchronization and spin-orbit alignment of each component, as well as for circularization of the orbit. The evolutionary age is also shown.

A somewhat unexpected result is that the times of alignment predicted by theory are also significantly longer than the current age of the system: $\tau_{\text{align},1} = 6.4$ Gyr and $\tau_{\text{align},2} = 6.8$ Gyr (or $\log \tau_{\text{align},1} = 9.804$ and $\log \tau_{\text{align},2} = 9.832$, in reference to Figure 9). At face value this indicates both spin axes may be inclined relative to the axis of the orbit, which is the opposite of what is almost universally assumed for binary systems. The long orbital period of LV Her could provide a plausible explanation, in principle, but in any case the misalignment makes it somewhat problematic to interpret the apparent lack of (pseudo-)synchronization inferred from the measured $v \sin i$, since the projection factor can no longer be assumed to be known.

The calculations above involve a number of approximations implicit in the equations we have used, as described, e.g., by Zahn (1977) and Hut (1981). In particular, they are linearized around the equilibrium state, and are strictly valid only for relatively small eccentricities and near-synchronous rotation, and for small relative inclinations between the spin axes and the axis of the orbit. We have also ignored changes in the semimajor axis that occur concurrently with the evolution of other orbital elements. The condition on the eccentricity is most certainly not met for LV Her ($e \simeq 0.613$), and it is unclear a priori to what extent this may affect the conclusions above. This, and the potentially interesting situation regarding the spin axes, have prompted us to explore the situation in greater detail. We have directly integrated the more general differential equations (valid also for high eccentricities) that describe the evolution of the semimajor axis (da/dt), eccentricity (de/dt), angular rotational rates ($d\Omega_1/dt$, $d\Omega_2/dt$), and inclination of the spin axes relative to the orbital axis ($d\Delta i/dt$ in our nomenclature) as given by Hut (1981), using a fourth-order Runge-Kutta method. Because they are coupled, these equations must be integrated simultaneously, and as before the stellar properties have been interpolated from the evolutionary tracks at each time step. The turbulent dissipation timescale for stellar phases with convective envelopes is taken to be $(MR^2/L)^{1/3}$, where M , R , and L are the mass, radius, and luminosity of the star. For phases with radiative envelopes the timescales adopted follow closely those in eq.(17) and eq.(18) by Claret & Cunha (1997).

The initial conditions are of course not known, so we explored a range of values that give predictions matching the observed quantities at the current age of the system. This is shown in Figure 10a,b for the eccentricity and orbital period. The initial values are $e_0 = 0.66$ and $P_0 = 21.8$ days at the starting age of $\log \tau_0 = 7.0$. According to these calculations we expect the orbit to circularize at an age $\log \tau_{\text{circ}} \simeq 9.85$ ($\tau_{\text{circ}} \simeq 7.1$ Gyr), which is in fairly good agreement with our previous estimate despite the concerns expressed above.

Also shown in the figure is the evolution of the angular rotation rate $\Omega = 2\pi/P_{\text{rot}}$ for each star, which we normalize for convenience to the orbital rate $\Omega_{\text{orb}} = 2\pi/P_{\text{orb}}$ (Figure 10c,d; solid lines). For LV Her we have no observational constraints on Ω_1 and Ω_2 , so the initial values are arbitrary and chosen to be the same. In principle they could be constrained by directly measuring the rotation periods of the stars due, e.g., to rotational modulation by

spots, although in practice this is difficult for a spatially unresolved binary. More importantly, these stars may be too hot to be affected significantly by spots. The ratio between the pseudo-synchronous velocity and the mean orbital motion is shown in Figure 10e, and this curve is repeated in Figure 10c,d (dot-dashed line). As seen from the convergence of the dot-dashed and solid curves, the stars are predicted to reach pseudo-synchronization roughly at $\log \tau_{\text{psync}} \simeq 8.75$ ($\tau_{\text{psync}} \simeq 0.6$ Gyr), which is much younger than the evolutionary age. This is completely at odds with our previous estimate, showing the limitations of that approach for a system like LV Her.

We also have no direct constraint on the relative angle Δi between the spin axes and the orbital axis. Furthermore, the relation between Δi and the orbital and rotational inclinations i_{orb} and i_{rot} , both measured relative to the plane of the sky, is given by

$$\cos \Delta i = \cos i_{\text{orb}} \cos i_{\text{rot}} + \sin i_{\text{orb}} \sin i_{\text{rot}} \cos \lambda, \quad (1)$$

which involves an unknown angle λ between the sky-projected angular momentum vectors of the orbit and the stellar spin.

The spectroscopically measured projected rotational velocities of the stars, which we refer to more properly now as $v \sin i_{\text{rot}}$, do provide some indirect constraint on a combination of the theoretically predictable quantities, but this still involves the unknown angle λ . Because i_{orb} is very nearly 90° for LV Her (see Table 8), we may make the approximation $\cos \Delta i \approx \sin i_{\text{rot}} \cos \lambda$. We then have

$$v_{1,2} \sin i_{\text{rot}} \approx \frac{2\pi}{P_{\text{orb}}} \frac{\Omega_{1,2}}{\Omega_{\text{orb}}} \frac{\cos \Delta i}{\cos \lambda} R. \quad (2)$$

In this equation all quantities on the right-hand side are either known from stellar evolution calculations (R), or can be computed from the solution of the differential equations, except for $\cos \lambda$, which depends on the observer's viewpoint. For the sake of illustration, we ignore this term in the following (or consider λ to be small), so that $\cos \Delta i \approx \sin i_{\text{rot}}$. In Figure 10f we show the evolution of Δi for four different initial values (20° , 40° , 60° , 80°). Curves for the primary and secondary are nearly indistinguishable, so we show only those for the primary. Once again the conclusion is very different from the one we reached with the equations by Zahn: alignment of the spin axes with the orbital axis is achieved much earlier than the age of the system, at $\log \tau_{\text{align}} \simeq 8.9$ (or $\tau_{\text{align}} \simeq 0.8$ Gyr). The corresponding $v \sin i_{\text{rot}}$ curves for the primary and secondary, calculated using eq.(2), are shown in the bottom panels and are compared with the measured rotations (dashed line and shaded uncertainty region). The general trend is for the stars in LV Her to be spun up by tidal forces, but the calculations disagree with the observations at the current age of the system, predicting the measured rotations should be 16 km s^{-1} for the primary and 15.5 km s^{-1} for the secondary (see also Table 8).⁴ These are nominally outside of the range allowed by the observational uncertainties. We consider it very unlikely that our measurements are off by as much

⁴ Although the rotation rates Ω_1 and Ω_2 have been chosen arbitrarily here, this does not affect the predicted rotational velocities at the current age because pseudo-synchronization occurs much earlier, independently of the starting values of Ω_1 and Ω_2 .

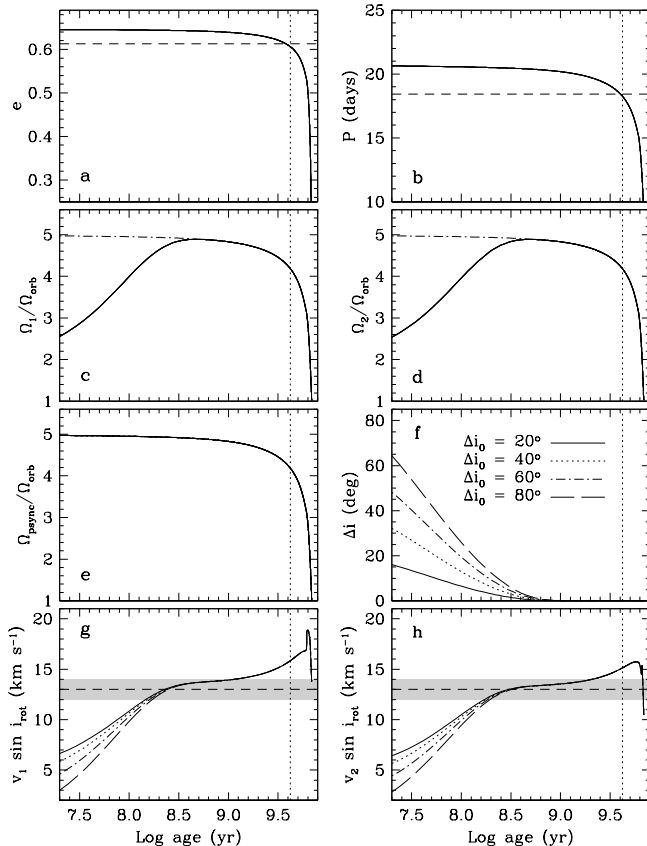


FIG. 10.— Observations of LV Her compared against tidal theory (Hut 1981). (a) Eccentricity evolution. The dashed line represents the measured value, and the vertical dotted line in this and the other panels marks the current evolutionary age of 4.2 Gyr, according to the models by Claret (2004). (b) Evolution of the orbital period, with the current value represented with a dashed line. (c) Rotation rate of the primary, normalized to the orbital rate. The dot-dashed line represents the evolution of the pseudo-synchronous rate shown in panel (e). (d) Same as (c), for the secondary. (e) Evolution of the pseudo-synchronous rotation rate. (f) Evolution of the relative angle Δi between the spin axis and the orbital axis, for different initial values. (g) Evolution of the projected rotational velocity of the primary, for the same four trial values of Δi . The dashed line represents the measured value, its uncertainty indicated by the shaded area. (h) Same as (g), for the secondary.

as 3 km s^{-1} for the primary and 2.5 km s^{-1} for the secondary, since our formal uncertainty of $\pm 1 \text{ km s}^{-1}$ is already conservative. The alternative would be a deficiency in the calculations, related to remaining approximations in the differential equations for this very challenging problem. A combination of both effects is also possible. An even more general treatment of the dynamical problem of tidal friction in binary systems with deformable components has been developed by Alexander (1973), but the application is considerably more complex and is beyond the scope of the present work.

We note, finally, that an empirical test of the prediction of alignment in eclipsing binaries by measuring the Rossiter-McLaughlin effect (e.g., Albrecht et al. 2007; Albrecht 2008). This provides a direct measure of the angle λ between the sky projections of the spin axes and the axis of the orbit.

6. DISCUSSION AND CONCLUSIONS

As a result of our intensive spectroscopic and photometric monitoring, the absolute masses and radii of

LV Her are now determined to 0.9% or better, and are among the best available for any eclipsing binary. In addition we have established the effective temperatures, as well as the overall metallicity. The latter quantity has not been determined for many eclipsing binaries, and is important because it reduces the degrees of freedom in the comparison with theory. Unfortunately the precision of $[m/H]$ (and T_{eff} to some extent) is limited in this case by poor knowledge of interstellar extinction in the direction of the star. This could perhaps be remedied with additional absolute photometric observations. Nevertheless, the combination of M , R , T_{eff} , and $[m/H]$ provides unusually strong constraints on stellar evolution theory. Comparison with current models yields an excellent fit to the observations, and indicates the stars are approximately half way through their main-sequence phase, at an age between 3.8 and 4.2 Gyr, depending on the model.

Eclipsing binaries with periods as long as that of LV Her are relatively rare and difficult to find, except perhaps in the course of automated variability surveys such as those designed to search for transiting planets, which often operate almost continuously for weeks or months at a time. The very high eccentricity of the system ($e \simeq 0.613$) makes it the most extreme case among those with well-determined properties (Torres et al. 2009). Although apsidal motion is expected, the apsidal period is predicted to be very long ($U \sim 58,000 \text{ yr}$) on account of the wide separation between the stars; it may take decades for the effect to be detected and measured accurately.

Tidal theory is consistent with the observations in predicting that the orbit should not yet have been circularized by tidal forces. Direct integration of the coupled differential equations for this problem according to Hut (1981) indicates that the spin axes have already been forced into alignment with the orbital axis early on in the evolution of this system. The spins of both stars are also expected to be pseudo-synchronized with the orbital motion, although this is not quite in agreement with the measured rotations, and may indicate either large errors of measurement (which we believe are unlikely) or shortcomings in theory, or some combination of both. The case of LV Her highlights the importance of bearing in mind the assumptions under which the equations for tidal evolution have been derived. Because of their ease of use and simpler interpretation, the linearized equations by Zahn (1977) (see also Hut 1981; Claret & Cunha 1997) have occasionally been applied to binary systems that may violate those assumptions to some degree (namely, the requirement of small eccentricities and spin-orbit inclinations, and near-synchronous rotations). Exactly when and how the theory breaks down is difficult to predict. With its high eccentricity, LV Her is one such case, as we have demonstrated here by comparing the critical times from the simpler formulation with the results from the more general equations given by Hut (1981).

We are grateful to P. Berlind, M. Calkins, R. J. Davis, E. Horine, D. W. Latham, J. Peters, and J. Zajak for their help in gathering the spectroscopic observations of LV Her used in this work, and to R. J. Davis for maintaining the echelle database at CfA. GT acknowledges partial support for this research through NSF grant

AST-0708229. CHSL thanks Bill Neely who operates and maintains the NFO for our Consortium, and who handles preliminary processing and storage of the images. He also wishes to thank summer 2009 Arkansas REU student Chris Gong for her preliminary analysis of the URSA data. This research has made use of the SIMBAD database and the VizieR catalogue ac-

cess tool, both operated at CDS, Strasbourg, France, of NASA's Astrophysics Data System Abstract Service, and of data products from the Two Micron All Sky Survey (2MASS), which is a joint project of the University of Massachusetts and the Infrared Processing and Analysis Center/California Institute of Technology, funded by NASA and the NSF.

REFERENCES

- Albrecht, S. 2008, Stars and planets at high spatial and spectral resolution, PhD Thesis, Leiden University, The Netherlands
- Albrecht, S., Reffert, S., Snellen, I., Quirrenbach, A., & Mitchell, D. S. 2007, *A&A*, 474, 565
- Alexander, M. E. 1973, *Ap&SS*, 23, 459
- Brát, L., Zejda, M., & Svoboda, P. 2007, *B.R.N.O. Contrib.*, 34
- Casagrande, L., Portinari, L., & Flynn, C. 2006, *MNRAS*, 373, 13
- Claret, A., & Cunha, N. C. S. 1997, *A&A*, 318, 187
- Claret, A. 1998, *A&AS*, 131, 395
- Claret, A. 2000, *A&A*, 383, 1081
- Claret, A. 2004, *A&A*, 424, 919
- Claret, A. 2008, *A&A*, 482, 259
- Demarque, P., Woo, J.-H., Kim, Y.-C., & Yi, S. K. 2004, *ApJS*, 155, 667
- Diethelm, R. 2008, *IBVS*, No. 5837
- Droege, T. F., Richmond, M. W., & Sallman, M. 2006, *PASP*, 118, 1666
- Etzel, P. B. 1981, *Photometric and Spectroscopic Binary Systems* (Dordrecht: Reidel), 65
- Flower, P. J. 1996, *ApJ*, 469, 355
- González Hernández, J. I., & Bonifacio, P. 2009, *A&A*, 497, 497
- Grauer, A. D., Neely, A. W., & Lacy, C. H. S. 2008, *PASP*, 120, 992
- Hilditch, R. W. & Hill, G. 1975, *MNRAS*, 79, 101
- Hoffmeister, C. 1935, *AN*, 255, 401
- Høg, E., Fabricius, C., Makarov, V. V., Urban, S., Corbin, T., Wycoff, G., Bastian, U., Schwkendiek, P., & Wicenec, A. 2000, *A&A*, 355, L27
- Hübscher, J. 2005, *IBVS*, No. 5643
- Hübscher, J., Steinbach, H.-M., & Walter, F. 2008, *IBVS*, No. 5830
- Hut P. 1981, *A&A*, 99, 126
- Lacy, C. H. S. 2002, *IBVS*, No. 5357
- Lacy, C. H. S. 2003, *IBVS*, No. 5487
- Lacy, C. H. S. 2004, *IBVS*, No. 5577
- Lacy, C. H. S. 2006, *IBVS*, No. 5670
- Lacy, C. H. S. 2007, *IBVS*, No. 5764
- Lacy, C. H. S., Claret, A., & Sabby, J. A. 2004a, *AJ*, 128, 1840
- Lacy, C. H. S., Claret, A., Sabby, J. A., Hood, B., & Secosan, F. 2004b, *AJ*, 128, 3005
- Lacy, C. H. S., Hood, B., & Straughn, A. 2001, *IBVS*, No. 5067
- Lacy, C. H. S., Straughn, A., & Denger, F. 2002, *IBVS*, No. 5251
- Lacy, C. H. S., Torres, G., & Claret, A. 2008, *AJ*, 135, 1757
- Lacy, C. H. S., Torres, G., Claret, A., & Menke, J. L. 2006, *AJ*, 131, 2664
- Lacy, C. H. S., Torres, G., Claret, A., & Vaz, L. P. R. 2005, *AJ*, 130, 2838
- Latham, D. W. 1985, in *IAU Coll. 88, Stellar Radial Velocities*, eds. A. G. D. Philip & D. W. Latham (Schenectady: L. Davis), 21
- Latham, D. W. 1992, in *IAU Coll. 135, Complementary Approaches to Double and Multiple Star Research*, ASP Conf. Ser. 32, eds. H. A. McAlister & W. I. Hartkopf (San Francisco: ASP), 110
- Latham, D. W., Nordström, B., Andersen, J., Torres, G., Stefanik, R. P., Thaller, M., & Bester, M. 1996, *A&A*, 314, 864
- Latham, D. W., Stefanik, R. P., Torres, G., Davis, R. J., Mazeh, T., Carney, B. W., Laird, J. B., & Morse, J. A. 2002, *AJ*, 124, 1144
- Perry, C. L., & Johnson, L. 1982, *ApJS*, 50, 451
- Perryman, M. A. C., et al. 1997, *The Hipparcos and Tycho Catalogues* (ESA SP-1200; Noordwijk: ESA)
- Popper, D. M. 1996, *ApJS*, 106, 133
- Popper, D. M. 1980, *ARA&A*, 18, 115
- Popper, D. M., & Etzel, P. B. 1981, *AJ*, 86, 102
- Ramírez, I., & Meléndez, J. 2005, *ApJ*, 626, 465
- Schlegel, D. J., Finkbeiner, D. P., & Davis, M. 1998, *ApJ*, 500, 525
- Selman F. J. 2004, *Optimizing Scientific Return for Astronomy through Information Technologies*, *Proc. SPIE*, 5493, 453
- Southworth, J., Bruntt, H., & Buzasi, D. L. 2007, *A&A*, 467, 1215
- Torres, G. 2000, *IBVS* No. 4971
- Torres, G., Andersen, J., & Giménez, A. 2009, *A&A Rev.*, in press
- Torres, G., Andersen, J., Nordström, B., & Latham, D. W. 2000a, *AJ*, 119, 1942
- Torres, G., Lacy, C. H. S., Claret, A., & Sabby, J. A. 2000b, *AJ*, 120, 3226
- Torres, G., Lacy, C. H. S., Guilbault, P. R., Diethelm, R., Baldwin, M. E., & Lubcke, G. C. 2001, *IBVS* No. 5201
- Torres, G., Neuhäuser, R., & Guenther, E. W. 2002, *AJ*, 123, 1701
- Torres, G., Stefanik, R. P., Andersen, J., Nordström, B., Latham, D. W., & Clausen, J. V. 1997, *AJ*, 114, 2764
- van Hamme, W. 1993, *AJ*, 106, 2096
- Yi, S. K., Demarque, P., Kim, Y.-C., Lee, Y.-W., Ree, C. H., Lejeune, T., & Barnes, S. 2001, *ApJS*, 136, 417
- Zahn, J.-P. 1977, *A&A*, 57, 383
- Zahn, J.-P. 1989, *A&A*, 220, 112
- Zessewitsch, V. P. 1944, *Astron. Circ.*, 36, 5
- Zessewitsch, V. P. 1954, *Odessa Report*, 4, 113
- Zucker, S., & Mazeh, T. 1994, *ApJ*, 420, 806